JACS
JOURNAL OF THE AMERICAN CHEMICAL SOCIETY

COMMUNICATION

pubs.acs.org/JACS

Anomalous Electronic Transport in Dual-Nanostructured Lead Telluride

J. Q. He,[*,†,‡] J. R. Sootsman,[‡] L. Q. Xu,[||] S. N. Girard,[‡] J. C. Zheng,[*,||] M. G. Kanatzidis,[*,‡] and V. P. Dravid[*,†]

[†]Department of Materials Science and Engineering and [‡]Department of Chemistry, Northwestern University, Evanston, Illinois 60208, United States

[||]Department of Physics, Institute of Theoretical Physics and Astrophysics, and Fujian Provincial Key Laboratory of Theoretical and Computational Chemistry, Xiamen University, Xiamen 361005, P. R. China

Supporting Information

ABSTRACT: The Pb- and Sb- dual nanostructured PbTe system exhibits anomalous electronic transport behavior wherein the carrier mobility first increases and then decreases with increase in temperature. By combining in situ transmission electron microscopy observations and theoretical calculations based on energy filtering of charge carriers, we propose a plausible mechanism of charge transport based on interphase potential that is mediated by interdiffusion between coexisting Pb and Sb precipitates. These findings promise new strategies to enhance thermoelectric figure of merit via dual and multinanostructuring of miscible precipitates.

Thermoelectric materials, which reversibly convert thermal energy into electrical power, will likely play increasingly important role in clean and renewable energy.[1−11] An efficient thermoelectric material must exhibit a high thermoelectric figure of merit, $ZT = (S^2\sigma/\kappa)T$, wherein, S is the Seebeck coefficient or thermopower, σ is the electrical conductivity, T is the absolute temperature, and κ is the total thermal conductivity.[2,3] This naturally leads to two conventional ways to improve ZT of the thermoelectric material: (i) enhance the power factor ($S^2\sigma$), and (ii) lower the thermal conductivity. The examples of the former approach include introduction of highly mismatched isoelectronic doping[2] or changing the density of state by resonance levels in the valence band.[4]The latter approach utilizes nanostructured materials to lower the thermal conductivity through phonon scattering by nanoscale features, interfaces, and defects,[5−9] and these reductions can approach the ultimate amorphous limit for thermal conductivity.[12] Hence, it is essential to balance the desirable reduction in thermal conductivity and minimize reduction in the carrier mobility for further improvements in thermoelectric performance.[5,6]

Most of the past studies, however, have typically been limited to one type of nanostructure. Herein, we report a synergistic effect of Pb and Sb dual-nanostructuring not only to lower the lattice thermal conductivity by enhancing phonon scattering[7] but also to increase the high temperature power factor to obtain high thermoelectric figure of merit.[10] By integrating in situ transmission electron microscopy (TEM) and theoretical calculations we find this intriguing synergistic effect may originate from suppression of interfacial potential mediated by interdiffusion between Pb and Sb when they coexist in close proximity, resulting in the anomalous electronic transport behavior in such systems. We believe this new dynamic approach and transport mechanism may fundamentally guide further improvement in the thermoelectric power factor for nanostructured thermoelectric systems, thereby potentially resolving the dichotomy between high power factor and low thermal conductivity which is often present in single nanostructured thermoelectric systems.

The synthesis methods and transport property measurements of all the n-type PbTe based thermoelectric materials investigated in this study can be found in our prior publication.[10] The in situ TEM experiments were carried out in a JEOL 2100F FasTEM microscope equipped with a heating stage (Gatan Corp.).[7,8] In Figure 1a electrical conductivity data from three main samples PbTe-Pb 0.5%-Sb 2% (Pb0.5Sb2), PbTe-Pb 1%-Sb 2% (Pb1Sb2) and PbTe-Pb 2%-Sb 3% (Pb2Sb3) taken between 300 and 750 K reveal a very different temperature dependence compared to that of PbTe nanostructured either with Sb or Pb nanodots (PbTe-Pb 2%(Pb2) and PbTe-Sb 3%(Sb3)). Although Pb0.5Sb2 composition is quite similar to that of Pb2 and Sb3 samples without any unusual electrical behavior, for Pb1Sb2 the electrical conductivity remained constant from 300 to 450 K and fell only very slowly from 450 to 675 K. Remarkably, for Pb2Sb3, the high room-temperature electrical conductivity of approximately 950 S cm^{-1} actually increased with increasing temperature, reaching about 1100 S cm^{-1} at 450 K before it started to fall, albeit very slowly, to approximately 600 S cm^{-1} at 700 K. Such changes in temperature dependence of the conductivity imply a significant change in how electrons (carriers) transport at these temperatures (Supporting Information [SI], Figure S1).

This anomalous temperature dependence of the conductivity in the dual-nanostructured PbTe samples cannot be attributed to a change in carrier concentration which is constant as determined by the Hall effect and Seebeck coefficient measurements (SI, Figure S1).[10] Normally, when Sb or Pb dissolve (see later) in the PbTe matrix with increasing temperature, the electron concentration should increase (i.e., n-type dopants). However it is known that in the presence of excess Pb, some antimony can be forced to occupy Te positions in PbTe, thereby becoming a p-type dopant, which will create holes.[11] Therefore, the observed constant carrier concentration is likely due to this carrier sign

Received: January 22, 2011
Published: May 10, 2011

dx.doi.org/10.1021/ja2006498 | J. Am. Chem. Soc. 2011, 133, 8786–8789

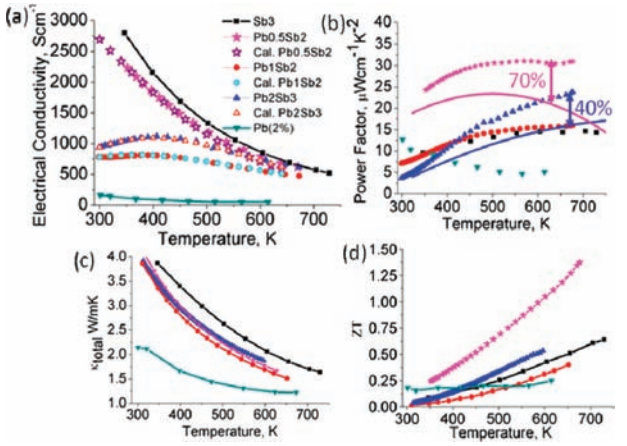

Figure 1. Temperature-dependent charge transport measurements and corresponding calculations of electrical conductivity (a), power factor (b), thermal conductivity (c), and ZT (d) for five samples Pb2, Sb3, Pb0.5Sb2, Pb1Sb2, and Pb2Sb3. In (b) Pb0.5Sb2 and Pb2Sb3 showing around 70% and 40% increase at 700 K compared to their conventional PbTe with the same carrier concentration.

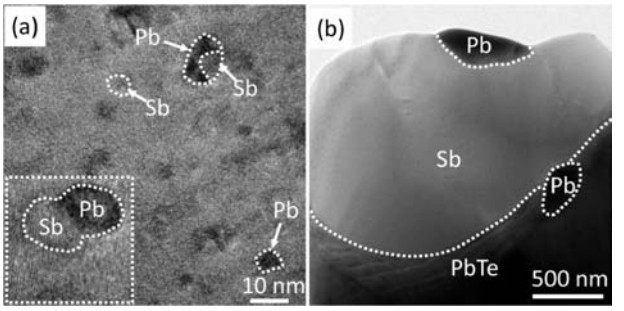

Figure 2. Typical images of the sample Pb1Sb2. The images show two types of precipitates: (a) nanoscale regime and (b) microscale regime.

competition. More n carriers are created with Pb dissolving in the PbTe matrix, but at the same time approximately equal holes are also created with Sb occupying Te sites in the PbTe matrix.[11] This *slow rate of decrease* in electrical conductivity in the dual-nanostructured PbTe samples gives rise to a much higher power factor at elevated temperatures as shown in Figure 1b. It shows two sets of samples; Pb0.5Sb2 and Pb2Sb3, with respective carrier concentration of 3×10^{19} cm^{-3} and 6×10^{19} cm^{-3}, exhibiting 70% and 40% increase in power factor at 700 K compared to the conventional PbTe with the same carrier concentration. The plots of the total thermal conductivity of all the samples (Figure 1c) show the three dual-nanostructured samples have trends similar to those of the Sb3 sample, and much higher than those of the Pb2 sample. The measured ZT values in Figure 1d represent a notable and significant increase compared to those of similarly doped PbTe, and the enhancement comes from the power factor.

In order to investigate the microstructural basis for the power factor enhancement, TEM measurements were conducted to assess the presence and extent of nanostructures. The TEM results of the three PbTe-based samples show nanoscale- and microscale precipitates in all specimens. The presence of microscale precipitates is further confirmed by X-ray data (SI, Figure S2). The nanoscale

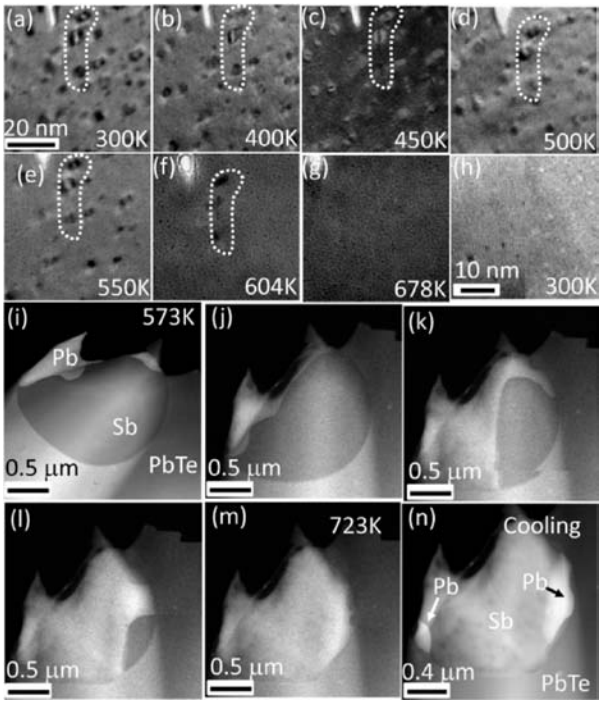

Figure 3. Temperature-dependent TEM/STEM images of the Pb1Sb2 sample. Images (a−g) focus on small precipitates which have the same magnification. The bright spot at the top left of the image is a result of intentional electron damage to track the location of the sample during heating. Image (h) showing some precipitates again after cooling down to room temperature. Images (i−n) concentrate on one large precipitate with Sb and Pb, which show the Pb melting and diffusing into Sb precipitate. (n) Image after cooling to room temperature.

precipitates have notably higher population, $\sim 2 \times 10^{12}/cm^2$, but the microscale precipitates exhibit much lower density, $\sim 4 \times 10^{2}/cm^2$. Most precipitates in all the samples have a regular spherical morphology, except for a very few platelet-like nanoscale precipitates in some specimens. Figure 2 shows the typical low magnification images of the Pb1Sb2 sample. In Figure 2a we find precipitates with three types of contrast levels: mostly dark, gray, and dual dark/gray contrast. All three kinds of contrast are present in the precipitates, although generally, the number density of the first two types is higher than that of the third type. A combination of high-resolution TEM and energy dispersion X-ray spectroscopy (EDS) reveals that the dark and gray contrast precipitates are rich in Pb and Sb, respectively. When the particle has both dark and gray contrast, it means that Pb and Sb coexit in one precipitate. Figure 2b is a typical image of a sample with such a dark and gray contrast in one single precipitate. Subsequent EDS analysis determined that the composition of precipitates with a large gray part is rich in Sb, while the two small dark parts are rich in Pb, as labeled in Figure 2b.

In order to determine the stability of the Pb and Sb precipitates at high temperature, in situ TEM was performed using a heating stage. A constant heating rate of 10 deg/min was used, and TEM images were collected from room temperature to 678 K, Figure 3a−g. A reference hole was created by electron beam in the sample to accurately determine the location of the sample (bright spot in images). Initially, at room temperature a large number of precipitates are clearly observed. As the temperature is increased, the Pb-rich precipitates begin to melt and evaporate at approximately 398−448 K, which is much lower than the Pb bulk

dx.doi.org/10.1021/ja2006498 |*J. Am. Chem. Soc.* 2011, 133, 8786–8789

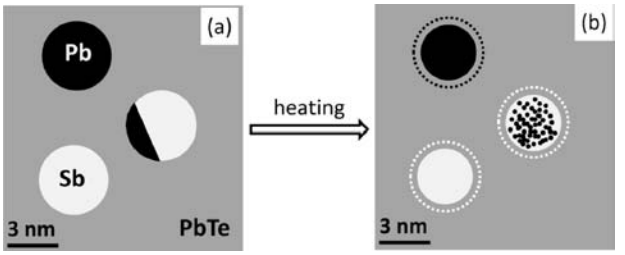

Figure 4. Schematic diagram of Pb and Sb nanoscale precipitates in the PbTe at room temperature and higher temperature.

melting temperature of 600 K and the Sb bulk melting temperature of 900 K.[13] At higher temperatures the precipitates continue to evaporate and start to dissolve, eventually completely disappearing at 678 K. The majority of the small precipitates disappeared most likely due to the thin-foil nature of the PbTe matrix samples, in addition to the presence of high vacuum and high vapor pressures of constituent elements. Yet, we believe that the nanoscale precipitates in this system should be stable at high temperature under operating (room atmosphere and bulk condition) detailed by SI, part A. When the high temperature specimen was cooled down to room temperature, some precipitates reappeared, as in Figure 3h. The dark contrast particles are Pb, and gray ones are Sb. However, compared to the precipitates before heating, their number density and size is reduced because of loss of mobile Pb/Sb atoms to the atmosphere during the experiment. The reappearance of the particles offers evidence that during the heating experiment a small portion of precipitates has diffused and dissolved into the PbTe matrix and another portion of Pb/Sb clearly evaporated from the very thin specimen.

Figure 3i−m shows scanning TEM (STEM) images from the heating sequence repeated on a larger precipitate. Figure 3i is an image taken at 573 K, which appears similar to that at room temperature. As shown, the large precipitate includes two parts: the small white area close to the edge is Pb-rich, and the other large darker region is Sb-rich, with the remaining sample being nominal matrix, PbTe. When the temperature is increased from 573 to 723 K (Figure 3j−m), the dark contrast region (defined as Sb) changes to lighter contrast starting from the Pb region, and finally the big precipitate becomes entirely of white contrast. This suggests that Pb begins to diffuse into Sb and also the whole Sb particle. As shown in Figure 3m, after the sample is cooled to 573 K, the Pb particles reappear. While one precipitate is at its original position, the other has diffused through the Sb particle to get to the interface between the Sb particle and PbTe matrix. EDS showed that the part labeled as "A" is still predominantly Sb-rich, and the brighter region is predominantly Pb-rich. These observations corroborate with expectation that liquid Pb can readily diffuse into solid or liquid Sb, but has difficulty diffusing into the PbTe matrix. Such analogous diffusion of liquid Pb in Al was also observed by Dahmen and co-workers.[14]

Figure 4 shows the schematic illustration of the behavior of small precipitates before and after heating. There is a small shrinkage associated with Pb and Sb-rich precipitates during heating above 450K due to interdiffusion in the PbTe matrix. As illustrated in Figure 4b, the dotted lines outline the particle size before heating and the solid lines represent their outline at higher temperature. For precipitates containing both Sb and Pb, Pb appreciably diffuses into Sb after heating due to its higher diffusivity. This leads to conversion of PbTe-Pb interfaces to PbTe-Sb. Therefore, nominally Pb-rich precipitates become Sb-rich precipitates at the higher temperature. We presume similar effects to occur for smaller nanoscale precipitates in the samples as well.

Following the microstructure dynamics, there is a need for understanding the associated transport properties, particularly the observation of enhanced power factor (due to higher carrier mobility at elevated temperature). Here, we provide the brief theoretical basis for the observed electrical properties of the samples over the range of 300−700 K based on Boltzmann transport equation (BTE) and modified two-band Kane model (details in SI, Part B).[15] The electron conductivity, σ, can be given as follows:

$$\sigma = \frac{e^2}{m_c^0}\frac{(2m_d^0 K_B T)^{3/2}}{3\pi^2\hbar^3}\int_0^\infty \gamma\frac{(z)^{3/2}}{\gamma'(z)}\left(-\frac{\partial f}{\partial z}\right)\tau(z)\mathrm{d}z \quad (1)$$

where m_d^0 is density of states effective mass, f is the Fermi−Dirac distribution function, $z = E/(k_B T)$ is dimensionless variable, $\gamma(z) = z + bz^2$ ($b = k_B T/E_g$), m_c^0 is the effective conductivity mass, $z_F = E_F/(k_B T)$, and τ is the total relaxation time. The latter is estimated by integrating the relaxation times from various scattering mechanisms, which can be expressed by:

$$\frac{1}{\tau} = \frac{1}{\tau_{PO}} + \frac{1}{\tau_A} + \frac{1}{\tau_O} + \frac{1}{\tau_v} + \frac{1}{\tau_i} \quad (2)$$

where the first four terms: τ_{PO} (polar optical phonons), τ_A (deformation potential acoustic phonons), τ_O (deformation potential optical phonons) and τ_v (short-range potential of vacancies) are from bulk which have been extensively investigated.[15−18,20]

The last variable, τ_i, is due to scattering from the nanoscale precipitates, mainly from the interfaces between PbTe matrix and metal precipitates. Based on the energy filtering theory[17] and our TEM observations, it is given by:

$$\frac{1}{\tau_i} \cong c_{Pb}(E)Vb_{Pb}^2\frac{x_{Pb}}{R_{Pb}}E^{-3/2} + c_{Sb}(E)Vb_{Sb}^2\frac{x_{Sb}}{R_{Sb}}E^{-3/2} + c_{Pb}(E)Vb_{Pb}^2\frac{x_{inter}}{R_{Pb}}\exp(-\alpha T + \beta)E^{-3/2} \quad (3)$$

where the parameter $c(E)$ is the Born factor; Vb is the interface potential between matrix and the precipitates;[17,21] R is the radius of the nanoscale precipitates; x is the volume fraction and the subscript inter denotes the interdiffusion between Pb and Sb; α and β are fitting parameters. The first two terms in the above equation represent contributions from each type of nanoscale precipitates, based on the theory of nanoscale precipitate scattering.[17] The third term accounts for the effects of interdiffusion between two nanoscale precipitates of different types (see, e.g., Figure 4). For two nanoscale precipitates close to each other, electrons are scattered by interface potential induced by such combined nanoscale precipitates.

As discussed previously, there is significant interdiffusion of Pb and Sb at elevated temperature. The electron scattering in these regions will be governed by complicated mechanisms, including some effects from the temperature-modified interface potential. In order to take into account some of the effects of interdiffusion, we have constructed an approximate model for "interdiffusion scattering" assuming decreasing interface potential (following the third term in the above equation) when temperature increases. For all samples, besides the parameters mentioned in SI, part B, three parameters, α, β, and x_{inter} are

dx.doi.org/10.1021/ja2006498 |J. Am. Chem. Soc. 2011, 133, 8786–8789

optimized by fitting the experiment data. For Pb0.5Sb2, very small interdiffusion effects are included. However, for samples Pb1Sb2 or Pb2Sb3, the interdiffusion term has to be considered in order to achieve a good fit, and we obtained $\alpha = 0.006$, $\beta = 1.8$ for both samples, and $x_{inter} = 0.5\%$ for Pb1Sb2 and $= 0.8\%$ for Pb2Sb3. Without the inclusion of the interdiffusion term, it is not possible to obtain the unusual feature of the bump in the electrical conductivity data (Figure 1a); i.e., the increase in electrical conductivity has to be rationalized by invoking interdiffusion-induced potential change at the interfaces. This indicates that Pb with high interdiffusion in Sb can account for the unusual temperature dependence of the electrical conductivity.

The scattering calculations (open symbols in Figure 1a) are in good agreement with the measured experimental data, suggesting the important role of Pb/Sb interdiffusion in (enhancing) the electrical conductivity of these systems. The novel temperature dependence of the mobility mentioned above is related to the behavior of electrons at the interfaces between matrix and precipitates. The TEM results lead to the following hypothesis for the observed mobility behavior. At room temperature the PbTe matrix contains Pb- or Sb-rich precipitates as well as those which contain both Pb and Sb in appreciable amounts. It has been shown previously[7] that Pb precipitates significantly reduce the electron mobility. However, as the temperature increases the Pb portion in precipitates with both Sb and Pb (which can significantly reduce the mobility) begins to diffuse into the Sb precipitates, thereby increasing the Sb atom contribution to interfacial electron scattering. Since Sb-rich precipitates do not compromise the electron mobility as much as Pb-rich precipitates do, the Pb-induced electron scattering decreases, and the overall mobility increases. This would explain the observed bump (enhancement) in electron mobility in transport measurements, which are corroborated with the observed decrease in Pb contribution to interdiffusion. As the temperature increases further, the volume contribution of Sb and Pb attains stability and pseudoequilibrium consistent with phase stability, and the mobility falls as expected with increasing temperature. The theoretical calculations utilizing the temperature dependent structural characterization provide complementary and corroborating evidence for understanding the transport behavior of this promising PbTe composite.

In summary, in situ transmission electron microscopy analysis, transport measurements, and theoretical calculations of dual-nanostructured PbTe with Pb and Sb precipitates have been presented to understand the observed anomalous increase in electron mobility at elevated temperature. We propose that the mechanism of the unusual transport is related to the interdiffusion of Pb and Sb atoms between the coexisting precipitates, wherein Sb-rich interfaces (due to high diffusivity of Pb) notably reduce the electron scattering at such dual-nanostructured interfaces, thereby increasing charge mobility at elevated temperatures. The theoretical analysis based on such chemically diffuse interfaces is consistent with experimental transport measurements. There effects stimulate new scientific inquiries and ideas on designing even more efficient thermoelectric materials based on multiphase nanostructuring of thermoelectric matrices.

■ ASSOCIATED CONTENT

Supporting Information. This information is available free charge via the Internet at http://pubs.acs.org.

■ AUTHOR INFORMATION

Corresponding Author

Jiaqing-he@northwestern.edu (J.Q.H.); jczheng@xmu.edu.cn (J.C.Z.); m-kanatzidis@northwestern.edu (M.G.K.); v-dravid@northwestern.edu (V.P.D.)

■ ACKNOWLEDGMENT

These materials are based mainly upon work supported as part of the Revolutionary Materials for Solid State Energy Conversion, an Energy Frontier Research Center funded by the U.S. Department of Energy, Office of Basic Energy Science under award number DE-SC0001054. TEM work was performed in the NU*ANCE* Center at Northwestern University which is supported by NSF-NSEC, NSF-MRSEC, Keck Foundation, the State of Illinois, and Northwestern University. Work at Xiamen University was supported by SRFDP No. 20090121120028, and the NSF of Fujian Province, China (Grant No. 2009J01015).

■ REFERENCES

(1) Snyder, J. G.; Toberer, E. S. *Nat. Mater.* **2008**, *7*, 105.
(2) Lee, J. H.; Wu, J. Q.; Grossman, J. C. *Phys. Rev. Lett.* **2010**, *104*, 016602.
(3) (a) Kanatzidis, M. G. *Chem. Mater.* **2010**, *22*, 648. (b) Sootsman, J. R.; Chung, D. Y.; Kanatzidis, M. G. *Angew. Chem., Int. Ed.* **2009**, *48*, 8616.
(4) Heremans, J. P.; Jovovic, V.; Toberer, E. S.; Saramat, A.; Kurosaki, K.; Charoenphakdee, A.; Yamanaka, S.; Snyder, G. J. *Science* **2008**, *321*, 554.
(5) Androulakis, J.; Lin, C. H.; Kong, H. J.; Uher, C.; Wu, C. I.; Hogan, T.; Cook, B. A.; Caillat, T.; Paraskevopoulos, K. M.; Kanatzidis, M. G. *J. Am. Chem. Soc.* **2007**, *129*, 9780.
(6) Hsu, K. F.; Loo, S.; Guo, F.; Chen, W.; Dyck, J. S.; Uher, C.; Hogan, T.; Polychroniadis, E. K.; Kanatzidis, M. G. *Science* **2004**, *303*, 818.
(7) He, J. Q.; Sootsman, J.; Girard, S.; Zheng, J. C.; Wen, J. G.; Zhu, Y.; Kanatzidis, M. G.; Dravid, V. P. *J. Am. Chem. Soc.* **2010**, *132*, 8669.
(8) He, J. Q.; Girard, S. N.; Kanatzidis, M. G.; Dravid, V. P. *Adv. Funct. Mater* **2010**, *20*, 764.
(9) Kanishka, B.; He, J.; Zhang, Q.; Dravid, V. P.; Wang, G.; Uher, C.; Kanatzidis, M. *Nature Chem.* **2011**, *3*, 160.
(10) Sootsman, J.; Kong, H.; Uher, C.; D'Angelo, J.; Wu, C.-I.; Hogan, T. P.; Caillat, T.; Kanatzidis, M. G. *Angew. Chem., Int. Ed.* **2008**, *47*, 8618.
(11) Jaworski, C. M.; Tobola, J.; Levin, E. M.; Schmidt-Rohr, K.; Heremans, J. P. *Phys. Rev. B* **2009**, *80*, 125208.
(12) Cahill, D. G.; Watson, S.; Pohl, R. O. *Phys. Rev. B* **1992**, *46*, 6131.
(13) (a) Singh, A; Tsai, A. P. *Sadhana* **2003**, *28*, 63. (b) Coombes, J. *J. Phys. F: Met. Phys.* **1972**, *2*, 441.
(14) Dahmen, U.; Radetic, T.; Hagege, S.; Zhang, L.; Johnson, E. *Microsc. Microanal.* **2003**, *9* (Suppl. 2), 54.
(15) Ravich, Yu. I. ; Efimova, B. A.; Smirnov, I. A. *Semiconducting Lead Chalcogenides*; Plenum: New York, 1970.
(16) (a) Popescu, A.; Woods, L. M.; Martin, J.; Nolas, G. S. *Phys. Rev. B* **2009**, *79*, 205302. (b) Martin, J.; Wang, L.; Chen, L.; Nolas, G. S. *Phys. Rev. B* **2009**, *79*, 115311.
(17) Faleev, S. V.; Leonard, F. *Phys. Rev. B* **2008**, *77*, 214304.
(18) Vineis, C. J.; Harman, T. C.; Calawa, S. D.; Walsh, M. P.; Reeder, R. E.; Singh, R.; Shakouri, A. *Phys. Rev. B* **2008**, *77*, 235202.
(19) Zayachuk, D. M. *Semiconductors* **1997**, *31*, 173.
(20) Heremans, J. P.; Thrush, C. M.; Morelli, D. T. *J. Appl. Phys.* **2005**, *98*, 063703.
(21) Michaelson, H. B. *J. Appl. Phys.* **1977**, *48*, 4729.